Preconditioning Strategies and Conformal Discretizations Empowered by High-Order Projectors

URSI-B EMTS 2025, Bologna, 23–27 June

Preconditioning Strategies and Conformal Discretizations Empowered by High-Order Projectors

Johann Bourhis*(1), Adrien Merlini(1), and Francesco P. Andriulli(2)
(1) IMT Atlantique, Brest, France
(2) Politecnico di Torino, Turin, Italy

Abstract

We present novel discretization schemes for surface integral equations within the framework of high-order boundary element methods. To overcome major limitations in existing high-order techniques, this paper introduces three key contributions: (i) a new conformal testing based on high-order quasi-Helmholtz projectors ensures the adequate high-order convergence of the magnetic field integral equation; (ii) this strategy allows to properly discretize the combined field integral equation, resulting for the first time in a resonance-free high-order formulation; and (iii) an original Calderón-like preconditioner also based on high-order conformal testing stabilizes these formulations for low-frequency and dense-refinement scenarios. This guarantees the rapid convergence of iterative solvers while enabling the efficient use of high-order methods across a wide frequency range and dense-mesh scenarios. Numerical experiments are provided to showcase the effectiveness of our approach.

1 Introduction

Time-harmonic electromagnetic problems modeling scattering and radiation from perfectly electrically conducting (PEC) objects can be solved equivalently via the electric and magnetic field integral equations (EFIE and MFIE) in conjunction with the boundary element method (BEM) [1], away from resonance frequencies. In the BEM, the surface of the object is approximated by a mesh of geometrical elements on which are defined basis functions that serve to test the equations and expand their unknowns. For challenging scenarios, it is common to rely on high-order polynomial expansions for both the surface parametrization and the surface current's functional space, which accelerate the convergence to the physical solution as the mesh is refined [2]. Unfortunately, the gains that can be achieved by leveraging higher-order methods are often jeopardized by the intrinsic numerical issues that plague both the EFIE and MFIE as they potentially limit the accuracy of their solutions and slow down or even prevent their computation via iterative solvers [1]. In particular, on the one hand, the EFIE is known to suffer from both low-frequency and dense-refinement ill-conditioning breakdowns, which cause a loss of accuracy and deteriorate performance of iterative solvers when the frequency decreases at fixed discretization density, and when the discretization density increases at fixed frequency, respectively [1]. On the other hand, the MFIE does not suffer from these downsides when modeling simply connected geometries, but conformal testing of the identity operator present in its definition requires the definition of a suitable dual space [3]. Moreover, both the EFIE and MFIE suffer from numerical instabilities due to the presence of spurious resonance modes at certain frequencies that imply ill-posedness of the underlying discretization systems in the neighborhood of these frequencies [1,4].

This last issue is commonly tackled by solving a weighted sum of the EFIE and MFIE, that is free from spurious resonance modes and is known as the combined field integral equation (CFIE). This formulation however inherits the ill-conditioning breakdowns of the EFIE for which an additional stabilization strategy is therefore needed to cure that critical behavior [1]. In [5], a technique was presented that leverages quasi-Helmholtz projectors and Calderón identities to address all aforementioned issues. Regrettably, this strategy has only been applied to the lowest-order BEM discretization as it requires the use of dual elements, such as the Buffa-Christiansen functions [3], for which full extension to higher orders has yet never been proposed.

In the present contribution, we introduce for the first time a scheme to properly discretize the MFIE and CFIE with a novel conformal testing based on high-order quasi-Helmholtz projectors [6]. To encompass low-frequency and dense-refinement scenarios, we also propose a stabilization of these formulations that leverages a Calderón-like preconditioner for high-order [6]. Numerical experiments support that the resulting Calderón-CFIE is a wide frequency range and dense-refinement stable formulation at arbitrary order.

The paper is organized as follows: Section 2 introduces the background and notations. Section 3 defines the novel dual space transformation matrix that provides conformal discretization of the MFIE and CFIE, presented in Section 4 and Section 5, respectively. In Section 6, we introduce the new Calderón preconditioning formulations for the EFIE, MFIE and CFIE. Section 7 provides numerical validations and we conclude in Section 8.

2 Background and notations

We consider a closed, simply connected surface Γ modeling the boundary of a PEC object with unitary normal $\widehat{\boldsymbol{n}}$ that is

approximated by a mesh of curvilinear triangles. Solving the EFIE and MFIE provides the surface current density $\boldsymbol{J}$ induced by an incident time-harmonic electromagnetic field $(\boldsymbol{E}^{\text{inc}},\boldsymbol{H}^{\text{inc}})$. They read $\left(jk\,\mathscr{T}_{s,k}+(jk)^{-1}\,\mathscr{T}_{h,k}\right)\boldsymbol{J}=-\frac{1}{\eta}\widehat{\boldsymbol{n}}\times\boldsymbol{E}^{\text{inc}}$ and $\left(\frac{1}{2}\mathscr{I}-\mathscr{K}_k\right)\boldsymbol{J}=\widehat{\boldsymbol{n}}\times\boldsymbol{H}^{\text{inc}}$ respectively, where k is the wavenumber, η is the characteristic impedance, $\mathscr{I}$ is the identity operator and $\left(\mathscr{T}_{s,k}\boldsymbol{J}\right)(\boldsymbol{r})=-\widehat{\boldsymbol{n}}(\boldsymbol{r})\times\int_\Gamma G_k(\boldsymbol{r},\boldsymbol{r}')\boldsymbol{J}(\boldsymbol{r}')\,\mathrm{d}S(\boldsymbol{r}')$, $\left(\mathscr{T}_{h,k}\boldsymbol{J}\right)(\boldsymbol{r})=\widehat{\boldsymbol{n}}(\boldsymbol{r})\times\boldsymbol{\nabla}\int_\Gamma G_k(\boldsymbol{r},\boldsymbol{r}')\mathrm{div}_\Gamma\boldsymbol{J}(\boldsymbol{r}')\,\mathrm{d}S(\boldsymbol{r}')$ and $(\mathscr{K}_k\boldsymbol{J})(\boldsymbol{r})=\widehat{\boldsymbol{n}}(\boldsymbol{r})\times\text{p.v.}\int_\Gamma\boldsymbol{\nabla}G_k(\boldsymbol{r},\boldsymbol{r}')\times\boldsymbol{J}(\boldsymbol{r}')\,\mathrm{d}S(\boldsymbol{r}')$, with $G_k(\boldsymbol{r},\boldsymbol{r}')=\frac{e^{-jk|\boldsymbol{r}-\boldsymbol{r}'|}}{4\pi|\boldsymbol{r}-\boldsymbol{r}'|}$. To solve these equations, we start by approximating the solution $\boldsymbol{J}$ by an expansion of Graglia-Wilton-Peterson (GWP) basis functions of order p [2] denoted as $\{\boldsymbol{\psi}_n^{(p)}\}_{n=1}^{N_p}$. The EFIE is then tested using rotated GWP functions $\{\boldsymbol{n}\times\boldsymbol{\psi}_m^{(p)}\}_{m=1}^{N_p}$ to form the matrix system of size N_p that reads $\mathbf{T}_p\boldsymbol{j}_p=\boldsymbol{e}_p$, with $[\boldsymbol{e}_p]_m=-\eta^{-1}\langle\widehat{\boldsymbol{n}}\times\boldsymbol{\psi}_m^{(p)},\widehat{\boldsymbol{n}}\times\boldsymbol{E}^{\text{inc}}\rangle$ and $[\mathbf{T}_p]_{mn}=\langle\widehat{\boldsymbol{n}}\times\boldsymbol{\psi}_m^{(p)},(jk\,\mathscr{T}_{s,k}+\frac{1}{jk}\,\mathscr{T}_{h,k})\boldsymbol{\psi}_n^{(p)}\rangle$. We finally orthonormalize the basis functions, which yields [6]

$$\widetilde{\mathbf{T}}_p\widetilde{\boldsymbol{j}}_p=\widetilde{\boldsymbol{e}}_p\,, \tag{1}$$

with $\widetilde{\mathbf{T}}_p=\mathbf{G}^{-1/2}_{\boldsymbol{\psi}^{(p)},\boldsymbol{\psi}^{(p)}}\mathbf{T}_p\mathbf{G}^{-1/2}_{\boldsymbol{\psi}^{(p)},\boldsymbol{\psi}^{(p)}}$, $\widetilde{\boldsymbol{e}}_p=\mathbf{G}^{-1/2}_{\boldsymbol{\psi}^{(p)},\boldsymbol{\psi}^{(p)}}\boldsymbol{e}_p$ and $\boldsymbol{j}_p=\mathbf{G}^{-1/2}_{\boldsymbol{\psi}^{(p)},\boldsymbol{\psi}^{(p)}}\widetilde{\boldsymbol{j}}_p$ and where the Gram matrix associated with two sets of scalar functions (or vector fields) $\{f_m\}_{m=1}^M$ and $\{g_n\}_{n=1}^N$ (or $\{\boldsymbol{f}_m\}_{m=1}^M$ and $\{\boldsymbol{g}_n\}_{n=1}^N$) is denoted $\mathbf{G}_{f,g}\in\mathbb{R}^{M\times N}$ (or $\mathbf{G}_{\boldsymbol{f},\boldsymbol{g}}\in\mathbb{R}^{M\times N}$), with $\left[\mathbf{G}_{f,g}\right]_{mn}=\int_\Gamma f_m(\boldsymbol{r})g_n(\boldsymbol{r})\,\mathrm{d}S(\boldsymbol{r})$ and $\left[\mathbf{G}_{\boldsymbol{f},\boldsymbol{g}}\right]_{mn}=\int_\Gamma\boldsymbol{f}_m(\boldsymbol{r})\cdot\boldsymbol{g}_n(\boldsymbol{r})\,\mathrm{d}S(\boldsymbol{r})$.

3 Dual space transformation matrix

We first recall the definition of the normalized quasi-Helmholtz projectors in high-order

$$\mathbf{P}_p^{\widetilde{\Sigma}}=\widetilde{\boldsymbol{\Sigma}}_p(\widetilde{\boldsymbol{\Sigma}}_p^{\mathsf{T}}\widetilde{\boldsymbol{\Sigma}}_p)^{+}\widetilde{\boldsymbol{\Sigma}}_p^{\mathsf{T}}\,, \tag{2}$$

where "+" denotes the Moore-Penrose pseudoinverse, with normalized Star matrix

$$\widetilde{\boldsymbol{\Sigma}}_p=\mathbf{G}^{-1/2}_{\boldsymbol{\psi}^{(p)},\boldsymbol{\psi}^{(p)}}\mathbf{G}_{\mathrm{div}_\Gamma\boldsymbol{\psi}^{(p)},\sigma^{(p)}}\mathbf{G}^{-1/2}_{\sigma^{(p)},\sigma^{(p)}}\,, \tag{3}$$

where $\{\sigma_n^{(p)}\}_{n=1}^{S_p}$ are the discontinuous basis functions of order p which span the space of the surface divergence of GWP functions of order p [2,6]. Using these projectors—that we introduced recently [6]—we define the following dual-space transformation matrix

$$\widetilde{\boldsymbol{\Theta}}_{r,p}=\widetilde{\mathbf{G}}^{\text{mix}}_{r,p}-\mathbf{P}_r^{\widetilde{\Sigma}}\widetilde{\mathbf{G}}^{\text{mix}}_{r,p}\mathbf{P}_p^{\widetilde{\Sigma}}\,, \tag{4}$$

with the normalized mixed-Gram matrix

$$\widetilde{\mathbf{G}}^{\text{mix}}_{r,p}=\mathbf{G}^{-1/2}_{\boldsymbol{\psi}^{(r)},\boldsymbol{\psi}^{(r)}}\mathbf{G}_{\widehat{\boldsymbol{n}}\times\boldsymbol{\psi}^{(r)},\boldsymbol{\psi}^{(p)}}\mathbf{G}^{-1/2}_{\boldsymbol{\psi}^{(p)},\boldsymbol{\psi}^{(p)}}\,. \tag{5}$$

In the following, the basis functions $\{\boldsymbol{\psi}_m^{(r)}\}_{m=1}^{N_r}$ are chosen to span the GWP space of order $p+1$ complemented with some cell-based divergence-free functions of higher order, that form a space of order in between $p+1$ and $p+2$. Theoretical evidences show that the following formulations properly discretize the associated surface integral equations whenever the space of order r includes that subspace, for instance with $r=p+2$ [6].

4 High-order conformal testing of the MFIE

It is well-established that the MFIE has to be tested with a suitable set of dual basis functions to yield the expected convergence to the physical solution as the mesh is refined [3]. Lamentably, such technique has yet never been proposed for high-order discretization. In this work, we propose for the first time to test the MFIE with the functions $\{\boldsymbol{n}\times\boldsymbol{\psi}_m^{(r)}\}_{m=1}^{N_r}$ which are then mapped to dual functions via the dual-space transformation matrix (4). Hence, the proposed MFIE discretization is

$$\widetilde{\boldsymbol{\Theta}}_{r,p}^{\mathsf{T}}\widetilde{\mathbf{M}}_{r,p}\widetilde{\boldsymbol{j}}_p=\widetilde{\boldsymbol{\Theta}}_{r,p}^{\mathsf{T}}\widetilde{\boldsymbol{h}}_r\,, \tag{6}$$

with $\widetilde{\mathbf{M}}_{r,p}=\left(\frac{1}{2}\widetilde{\mathbf{G}}^{\text{mix}}_{r,p}-\widetilde{\mathbf{K}}_{r,p}\right)$, where $[\mathbf{K}_{r,p}]_{mn}=\langle\widehat{\boldsymbol{n}}\times\boldsymbol{\psi}_m^{(r)},\mathscr{K}_k\boldsymbol{\psi}_n^{(p)}\rangle$, $\widetilde{\mathbf{K}}_{r,p}=\mathbf{G}^{-1/2}_{\boldsymbol{\psi}^{(r)},\boldsymbol{\psi}^{(r)}}\mathbf{K}_{r,p}\mathbf{G}^{-1/2}_{\boldsymbol{\psi}^{(p)},\boldsymbol{\psi}^{(p)}}$, $[\boldsymbol{h}_r]_m=\langle\widehat{\boldsymbol{n}}\times\boldsymbol{\psi}_m^{(r)},\widehat{\boldsymbol{n}}\times\boldsymbol{H}^{\text{inc}}\rangle$ and $\widetilde{\boldsymbol{h}}_r=\mathbf{G}^{-1/2}_{\boldsymbol{\psi}^{(r)},\boldsymbol{\psi}^{(r)}}\boldsymbol{h}_r$.

5 High-order conformal testing of the CFIE

It is known that both the EFIE and MFIE suffer from the presence of resonance modes at some frequencies [1]. To mitigate these issues, we compute a weighted sum of the EFIE (1) and MFIE (6), that is effective only if conformal testings are employed for both equations. Setting $\alpha\in]0,1[$, the proposed CFIE formulation reads

$$\left(\alpha\widetilde{\mathbf{T}}_p-(1-\alpha)\widetilde{\boldsymbol{\Theta}}_{r,p}^{\mathsf{T}}\widetilde{\mathbf{M}}_{r,p}\right)\widetilde{\boldsymbol{j}}_p=\alpha\widetilde{\boldsymbol{e}}_p-(1-\alpha)\widetilde{\boldsymbol{\Theta}}_{r,p}^{\mathsf{T}}\widetilde{\boldsymbol{h}}_r\,, \tag{7}$$

which is free from spurious resonance modes but still suffers from low-frequency and dense-refinement ill-conditioning breakdowns [1].

6 Calderón preconditioners for high-order

To obtain wide frequency range and dense-refinement stable formulations, we derive original preconditioning schemes for the EFIE (1), MFIE (6) and CFIE (7) formulations compatible with high-order discretization. These are based on the Calderón identities which show—at least for sufficiently smooth geometries away from resonance frequencies—that we can leverage some compositions between surface integral operators to form operators having bounded spectra (see [1] and references therein). As in [5], the left matrices used as preconditioners are formed following a Yukawa-type strategy in that the wavenumber k is replaced by $-jk$ in the surface integral operators defining the preconditioning matrices. Therefore, we define the Calderón-EFIE formulation as

$$\widetilde{\boldsymbol{\Theta}}_{r,p}^{\mathsf{T}}\widetilde{\mathbb{T}}_r\widetilde{\boldsymbol{\Theta}}_{r,p}\widetilde{\mathbf{T}}_p=\widetilde{\boldsymbol{\Theta}}_{r,p}^{\mathsf{T}}\widetilde{\mathbb{T}}_r\widetilde{\boldsymbol{\Theta}}_{r,p}\widetilde{\boldsymbol{e}}_p\,. \tag{8}$$

with $[\mathbb{T}_r]_{mn}=\langle\widehat{\boldsymbol{n}}\times\boldsymbol{\psi}_m^{(r)},(jk\,\mathscr{T}_{s,-jk}+\frac{1}{jk}\,\mathscr{T}_{h,-jk})\boldsymbol{\psi}_n^{(r)}\rangle$ and $\widetilde{\mathbb{T}}_r=\mathbf{G}^{-1/2}_{\boldsymbol{\psi}^{(r)},\boldsymbol{\psi}^{(r)}}\mathbb{T}_r\mathbf{G}^{-1/2}_{\boldsymbol{\psi}^{(r)},\boldsymbol{\psi}^{(r)}}$. The Calderón-MFIE formulation is then defined as

$$\widetilde{\boldsymbol{\Theta}}_{r,p}^{\mathsf{T}}\widetilde{\mathbb{M}}_{r,p}\widetilde{\boldsymbol{\Theta}}_{r,p}^{\mathsf{T}}\widetilde{\mathbf{M}}_{r,p}=\widetilde{\boldsymbol{\Theta}}_{r,p}^{\mathsf{T}}\widetilde{\mathbb{M}}_{r,p}\widetilde{\boldsymbol{\Theta}}_{r,p}^{\mathsf{T}}\widetilde{\boldsymbol{h}}_r\,. \tag{9}$$

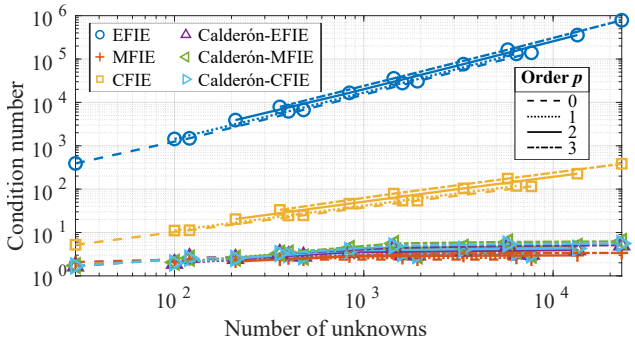

Figure 1. Condition numbers of the matrices associated with the different formulations as a function of the number of unknowns at fixed frequency $f = 100\,\text{MHz}$, for order $p \in \{0,1,2,3\}$. PEC sphere of radius 1 m.

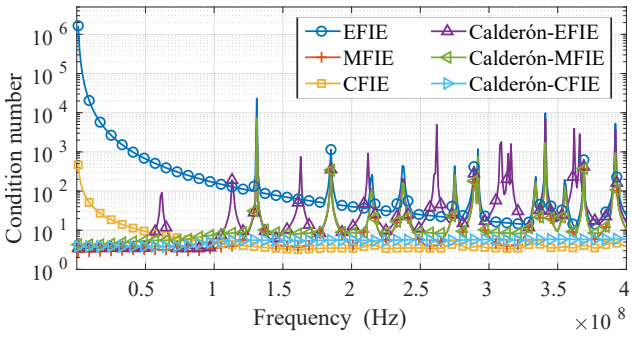

Figure 2. Condition numbers of the matrices associated with the different formulations as a function of the frequency, at fixed discretization (average edge size is $h = 0.58$ m and order is $p = 2$). PEC sphere of radius 1 m.

with $\widetilde{\mathbb{M}}_{r,p} = \left(\frac{1}{2}\widetilde{\mathbf{G}}^{\text{mix}}_{r,p} + \widetilde{\mathbb{K}}_{r,p}\right)$, where $[\mathbb{K}_{r,p}]_{mn} = \langle \widehat{\boldsymbol{n}} \times \boldsymbol{\psi}^{(r)}_m, \mathscr{K}_{-jk}\boldsymbol{\psi}^{(p)}_n \rangle$ and $\widetilde{\mathbb{K}}_{r,p} = \mathbf{G}^{-1/2}_{\boldsymbol{\psi}^{(r)},\boldsymbol{\psi}^{(r)}} \mathbb{K}_{r,p} \mathbf{G}^{-1/2}_{\boldsymbol{\psi}^{(p)},\boldsymbol{\psi}^{(p)}}$. Finally, the new high-order Calderón-CFIE formulation is

$$\begin{aligned} &\widetilde{\boldsymbol{\Theta}}^{\mathsf{T}}_{r,p}\widetilde{\mathbb{T}}_r\widetilde{\boldsymbol{\Theta}}_{r,p}\widetilde{\mathbf{T}}_p + \; j\widetilde{\boldsymbol{\Theta}}^{\mathsf{T}}_{r,p}\widetilde{\mathbb{M}}_{r,p}\widetilde{\boldsymbol{\Theta}}^{\mathsf{T}}_{r,p}\widetilde{\mathbf{M}}_{r,p} \\ &= \widetilde{\boldsymbol{\Theta}}^{\mathsf{T}}_{r,p}\widetilde{\mathbb{T}}_r\widetilde{\boldsymbol{\Theta}}_{r,p}\widetilde{\boldsymbol{e}}_p + \; j\widetilde{\boldsymbol{\Theta}}^{\mathsf{T}}_{r,p}\widetilde{\mathbb{M}}_{r,p}\widetilde{\boldsymbol{\Theta}}^{\mathsf{T}}_{r,p}\widetilde{\boldsymbol{h}}_r\,, \end{aligned} \tag{10}$$

which does not suffer from the presence of spurious resonance modes, in addition to be free from low-frequency and dense-refinement breakdowns, as in [5] at order zero.

7 Numerical validations

To validate the effectiveness of our approach, we evaluate the condition number of the matrices obtained for the EFIE (1), MFIE (6) and CFIE (7) formulations, as well as for their Calderón preconditioning counterparts (8), (9) and (10), respectively. For the CFIE, we set $\alpha = 0.2$. As indicated in Section 3, the order r defining the dual transformation matrix (4) refers to the GWP space of order $p+1$, complemented with the curl of bubble functions contained in the GWP space of order $p+2$. Tests are done for scattering simulations of the PEC sphere of radius 1 m illuminated by an incident plane wave $(\boldsymbol{E}^{\text{inc}}, \boldsymbol{H}^{\text{inc}}) = (\widehat{\boldsymbol{x}}e^{-jk\widehat{\boldsymbol{z}}\cdot\boldsymbol{r}}, \frac{-1}{\eta}\widehat{\boldsymbol{y}}e^{-jk\widehat{\boldsymbol{z}}\cdot\boldsymbol{r}})$, where $\{\widehat{\boldsymbol{x}}, \widehat{\boldsymbol{y}}, \widehat{\boldsymbol{z}}\}$ is the canonical basis in the Cartesian coordinates.

To start, we display in Figure 1 the condition number as a function of the number of unknowns (growing for increasing mesh density and increasing order) for $p \in \{0,1,2,3\}$. For every order, we observe that only the EFIE (1) and CFIE (7) formulations display condition numbers that increase with the number of unknowns, unlike the MFIE that does not suffer from dense-refinement breakdown, as expected from the theory [1]. We finally observe that the three Calderón preconditioning formulations (8), (9) and (10) do not suffer from these effects, which validates the effectiveness of the preconditioning approach to cure the dense-refinement breakdown of the EFIE and CFIE formulations.

Next, we display in Figure 2 the condition number as a function of the frequency for a fixed mesh density (with average edge size $h = 0.58$ m) and for $p = 2$, leading to matrix systems of size $N_p = 840$ and $N_r = 1680$. We observe two frequency-related behaviors of the different formulations. First, we see that both the EFIE (1) and CFIE (10) suffer from low-frequency breakdown as their condition numbers increase when the frequency approaches zero. Second, the condition numbers of the EFIE (1), MFIE (6), Calderón-EFIE (8) and Calderón-MFIE (9) increase in the neighborhood of some resonance frequencies while it is not the case for neither the CFIE (7) nor the Calderón-CFIE (10). Overall, only the Calderón-CFIE formulation (10) displays a condition number that is almost constant for any frequencies.

For the final experiments, we set $p = 2$ and $h = 0.32\,\text{m}$, leading to systems of size $N_p = 3360$ and $N_r = 6720$. For these discretization settings, we found $f = 340.7\,\text{MHz}$ as a frequency close enough to a resonance and $f = 330.0\,\text{MHz}$ as a frequency farther from resonance, where better conditioning is observed for every formulation. We then evaluated the number of iterations carried out by the solver TFQMR (with tolerance 10^{-6}) used to solve the different formulations at these two frequencies. To assess the accuracy of the solutions, we considered the relative error of the computed bistatic radar cross section (RCS) compared with the reference solution provided by the Mie series, which is evaluated at 395012 points located on a uniform spherical grid. These results are given in Table 1. We first observe that only the condition number and the number of iterations of the CFIE and Calderón-CFIE formulations remain almost constant for both frequencies. We then observe that the MFIE formulations are less accurate than the other formulations at frequency close to resonance. It is worth noting here that EFIE formulations are known to enable relatively accurate computation of the far field, despite the presence of resonance modes that however compromise the accuracy of their solutions and computed near fields [4]. To illustrate this latter point, we display in Figure 3 the surface current densities on the PEC surface for the two con-

		EFIE	MFIE	CFIE
330.0 MHz	**cond.**	6.9E1	1.6E1	4.4E0
	iter.	322	37	59
	err. RCS	1.2E-4	2.1E-4	1.8E-4
340.7 MHz*	**cond.**	9.3E4	8.0E4	3.9E0
	iter.	566	70	57
	err. RCS	1.2E-4	8.3E-2	2.0E-4
		C-EFIE	**C-MFIE**	**C-CFIE**
330.0 MHz	**cond.**	1.6E1	1.6E1	5.7E0
	iter.	69	45	24
	err. RCS	1.2E-4	2.1E-4	2.2E-4
340.7 MHz*	**cond.**	3.0E4	8.4E4	5.8E0
	iter.	110	82	24
	err. RCS	1.2E-4	9.2E-2	2.4E-4

Table 1. Condition number (cond.), number of iterations of TFQMR for a given tolerance 10^{-6} (iter.) and relative error of the bistatic RCS (err. RCS); for the EFIE (1), MFIE (6), CFIE (7), and their Calderón preconditioning counterparts C-EFIE (8), C-MFIE (9) and C-CFIE (10); at frequencies $f = 330.0\,\text{MHz}$ (farther from resonance) and $f = 340.7\,\text{MHz}$ (*close to resonance).

sidered frequencies and for the EFIE, MFIE and CFIE formulations (Calderón counterparts are omitted here as they provide similar observations). The EFIE does not yield the same solution as the CFIE at frequency close to resonance, which indicates that the EFIE solution is compromised by the presence of resonance modes [4]. The MFIE also yields a compromised solution, as expected from the computation of the bistatic RCS in Table 1. At frequency farther from resonance the three solutions appear to be almost identical.

8 Conclusion

We introduced novel formulations based on the discretization of surface integral equations with high-order basis functions. For the first time, a conformal testing has been employed to discretize the MFIE and CFIE in high-order. Calderón preconditioning strategies were also applied to the EFIE, MFIE and CFIE. The resulting Calderón-CFIE formulation does not suffer from low-frequency and dense-refinement breakdowns and is free from spurious resonances. It allows to significantly reduce the number of iterations of iterative solvers within a wide range of applications that are now able to benefit from high-order convergence.

Acknowledgment

This work was supported by the EU H2020 research and innovation programme under the Marie Skłodowska-Curie grant agreement n° 955476 (project COMPETE), by the European Innovation Council (EIC) through the European Union's Horizon Europe research Programme under Grant 101046748 (Project CEREBRO) and by the Institut Carnot Télécom et Société Numérique.

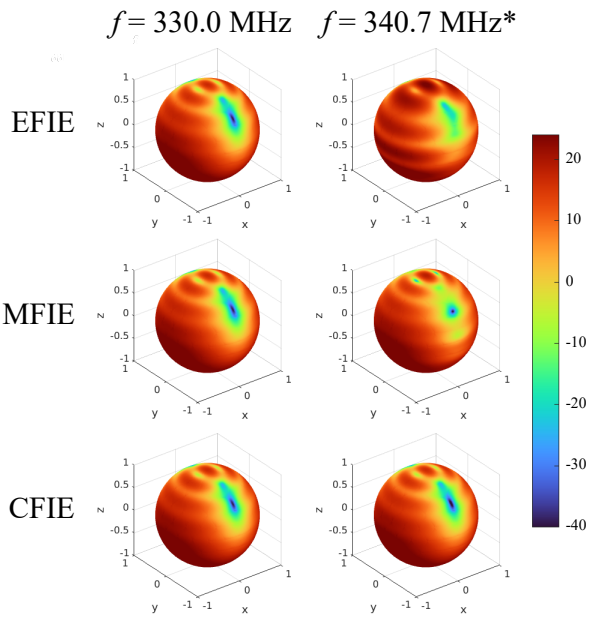

Figure 3. Amplitude of the surface current density (in $\text{dB}_{\text{A/m}}$) obtained as a solution of the EFIE (1), MFIE (6) and CFIE (7) at frequencies $f = 330.0\,\text{MHz}$ (farther from resonance) and $f = 340.7\,\text{MHz}$ (*close to resonance).

References

[1] S. B. Adrian, A. Dély, D. Consoli, A. Merlini, and F. P. Andriulli, "Electromagnetic Integral Equations: Insights in Conditioning and Preconditioning," *IEEE Open Journal of Antennas and Propagation*, vol. 2, pp. 1143–1174, 2021.

[2] R. Graglia, D. Wilton, and A. Peterson, "Higher Order Interpolatory Vector Bases for Computational Electromagnetics," *IEEE Transactions on Antennas and Propagation*, vol. 45, no. 3, pp. 329–342, 1997.

[3] K. Cools, F. P. Andriulli, D. De Zutter, and E. Michielssen, "Accurate and Conforming Mixed Discretization of the MFIE," *IEEE Antennas and Wireless Propagation Letters*, vol. 10, pp. 528–531, 2011.

[4] S. Christiansen, "Discrete Fredholm Properties and Convergence Estimates for the Electric Field Integral Equation," *Math. Comput.*, vol. 73, pp. 143–167, 01 2004.

[5] A. Merlini, Y. Beghein, K. Cools, E. Michielssen, and F. P. Andriulli, "Magnetic and Combined Field Integral Equations Based on the Quasi-Helmholtz Projectors," *IEEE Transactions on Antennas and Propagation*, vol. 68, no. 5, pp. 3834–3846, 2020.

[6] J. Bourhis, D. Franzò, A. Merlini, and F. P. Andriulli, "On a Novel Calderón Preconditioning Strategy Based on High-Order Quasi-Helmholtz Projectors," in *2024 International Conference on Electromagnetics in Advanced Applications (ICEAA)*, 2024, pp. 700–703.